BIOCHEMISTRY
including biophysical chemistry & molecular biology

Article

pubs.acs.org/biochemistry

Insights into Substrate Binding to the Oxygen-Evolving Complex of Photosystem II from Ammonia Inhibition Studies

David J. Vinyard and Gary W. Brudvig*

Department of Chemistry, Yale University, New Haven, Connecticut 06520-8107, United States

Supporting Information

ABSTRACT: Water oxidation in Photosystem II occurs at the oxygen-evolving complex (OEC), which cycles through distinct intermediates, S_0−S_4. The inhibitor ammonia selectively binds to the S_2 state at an unresolved site that is not competitive with substrate water. By monitoring the yields of flash-induced oxygen production, we show that ammonia decreases the net efficiency of OEC turnover and slows the decay kinetics of S_2 to S_1. The temperature dependence of biphasic S_2 decay kinetics provides activation energies that do not vary in control and ammonia conditions. We interpret our data in the broader context of previous studies by introducing a kinetic model for both the formation and decay of ammonia-bound S_2. The model predicts ammonia binds to S_2 rapidly ($t_{1/2}$ = 1 ms) with a large equilibrium constant. This finding implies that ammonia decreases the reduction potential of S_2 by at least 2.7 kcal mol^{-1} (>120 mV), which is not consistent with ammonia substitution of a terminal water ligand of Mn(IV). Instead, these data support the proposal that ammonia binds as a bridging ligand between two Mn atoms. Implications for the mechanism of O−O bond formation are discussed.

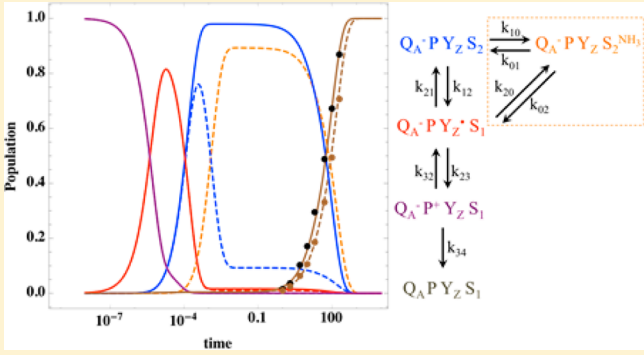

The Photosystem II (PSII) reaction center catalyzes the oxidation of water using solar energy, thus providing virtually all the molecular oxygen (O_2) on Earth.[1,2] This chemistry is performed at the oxygen-evolving complex (OEC), a $Mn_4CaO_5(H_2O)_4$ cluster embedded in the protein. Two water molecules are oxidized following four sequential hole transfers to the OEC from a conserved redox-active tyrosine residue (Y_Z) and the chlorophyll *a* primary electron donor, P_{680}. Thus, the OEC cycles through four distinct intermediates (S_0−S_3).[3] An S_4 intermediate is formed following the deprotonation and oxidation of S_3, which spontaneously evolves O_2, binds water, and re-forms S_0. Both S_2 and S_3 are metastable and decay in darkness to S_1.[4]

Ammonia has two binding sites on the donor side of PSII. The first is competitive with chloride and presumably is located in the second shell of residues around the OEC at or near the chloride-binding site (see Figure 1).[5−7] The second involves direct binding of chloride to manganese in the OEC in S_2,[6,8] thus altering the cluster's electronic properties.[5,8,9] Substituted amines do not bind to the OEC in S_2 but do bind to the chloride-competitive site.[5] It has also been shown that ammonia does not compete with a substrate water.[6,8,10,11] Therefore, by determining the mode of binding of ammonia to the OEC, we can eliminate that position as a substrate water-binding site and shed light on the mechanism of O−O bond formation.

Previous work on ammonia binding showed not only that S_2 exhibited an altered EPR "multiline" signal[8] but also that the intermediate had a lifetime substantially longer than that of normal S_2.[8,10,12−14] Thermoluminescence glow curves representing the $[S_2Q_A^-]$ and $[S_2Q_B^-]$ recombinations were shifted 15° and 12° higher, respectively, than controls.[14] These results

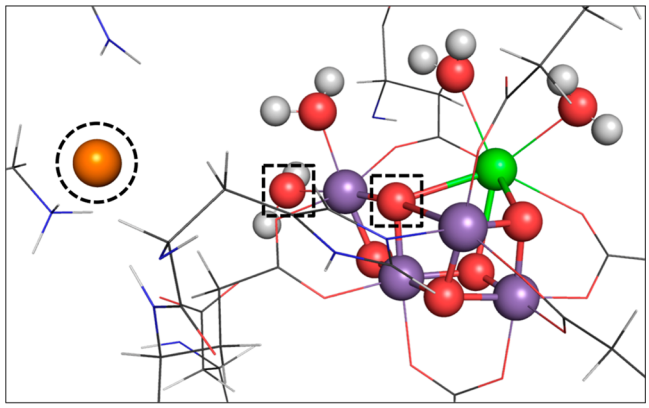

Figure 1. Structure of the OEC and local protein environment showing Mn (purple), Ca (green), chloride (orange), and oxygen (red). Ammonia binds to two sites: one site that is competitive with chloride (dashed circle) and a second site that is directly on Mn in the OEC (two proposed positions, W1 and O5, are shown with dashed squares). Image generated in PyMOL using coordinates computationally optimized for the S_1 state.[43]

Received: November 13, 2014
Published: December 22, 2014

DOI: 10.1021/bi5014134
Biochemistry 2015, 54, 622−628

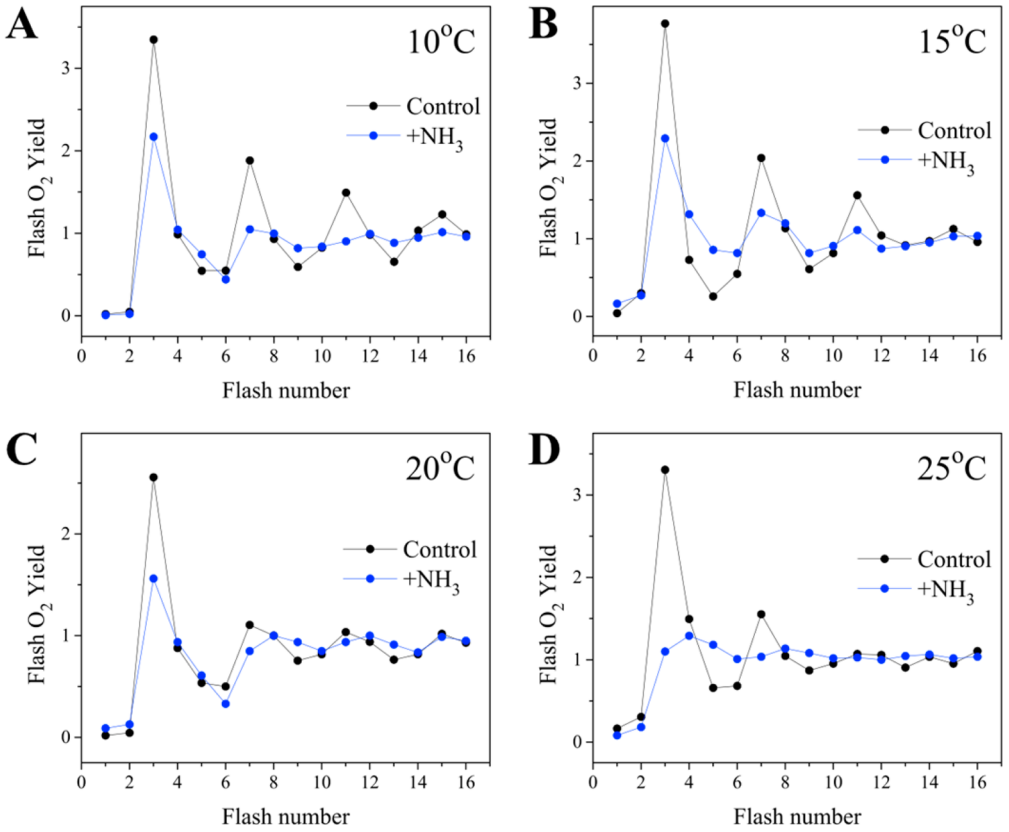

Figure 2. Flash O_2 yields in the absence (black) and presence (blue) of ammonia at (A) 10, (B) 15, (C) 20, and (D) 25 °C.

suggested that the S_2 reduction potential is lower when ammonia is bound.[12,14,15]

Spectroscopic evidence of the location and binding mode of ammonia bound to the OEC in S_2 remains inconclusive. For example, ESEEM experiments by Britt and co-workers tentatively assign ammonia as a bridging ligand.[9] This conclusion is consistent with FTIR measurements in the presence of ammonia[16] that showed the loss of a Mn−O−Mn stretch.[17] However, a terminal binding motif for ammonia was proposed in a recent study by Navarro and co-workers.[11] This study used X-band ESEEM to show that ammonia is a ligand to a Mn(IV) in S_2 and Q-band ^{1}H ENDOR to show that protons surrounding the OEC do not substantially change upon ammonia binding. In addition, W-band ^{17}O EDNMR experiments showed that ammonia binding narrows the spectral envelopes by ∼30% and alters their overall shapes. Only features from a ^{17}O of intermediate coupling strength (assigned as W2) remain clearly visible in both the control and ammonia-bound spectra. Both the strongly coupled ^{17}O (assigned to O5) and the weakly coupled ^{17}O (assigned to W1) are unresolved in the presence of ammonia. However, by using simulations that varied both the intensities and frequencies of the various components, the authors conclude that ammonia binds to the W1 site, thus altering the O5 environment.

Because substitution of ammonia for a terminal water would not have a substantial effect on the reduction potential of S_2, given the similar ligand field strengths of ammonia and water,[18] the conclusion that ammonia binds in place of W1 is at odds with the previously reported stabilization of S_2 when ammonia is bound. The experiments in this study seek to improve our understanding of the effect of ammonia on the OEC and its implications for the mechanism of photosynthetic water oxidation.

MATERIALS AND METHODS

PSII membranes were prepared from market spinach as previously described[19] with minor modifications[20] and stored at 77 K in a buffer containing 20 mM MES (pH 6.0), 15 mM NaCl, and 30% ethylene glycol. Samples were thawed on ice and washed three times by centrifugation and resuspension in 60 mM HEPES-NaOH (pH 7.5), 10 mM $Ca(OH)_2$, 60 mM NaCl, and 400 mM sucrose. Flash O_2 yields were measured polarographically using a bare platinum electrode with a silver counter electrode poised at −700 mV. Flashes were provided by an EG&G Xe flash lamp. A home-built controller interfaced to an Arduino Uno (Ivrea, Italy) board provided one flash followed by a variable delay time. Twenty flashes at 1 Hz were then applied. The resulting period-four oscillations in flash O_2 yield were analytically fit to the VZAD model using the BOBYQA nonlinear optimization algorithm.[21] The relative population of S_2 at the beginning of the 20-flash sequence was plotted as a function of delay time following the initial flash as previously described.[22,23] Data were fit to the biexponential decay function:

$$y = y_o + A_1 \exp(-x/\tau_1) + A_2 \exp(-x/\tau_2)$$

For each experiment, 25 μg of Chl (∼4 μM PSII) was supplemented with an additional 50 mM NaCl (control) or 50 mM NH_4Cl (0.9 mM NH_3 at pH 7.5). Note that the ammonia samples also contained 60 mM NaCl to prevent contributions from the chloride-dependent ammonia-binding site. $K_3Fe(CN)_6$ (1 mM) and PPBQ (0.25 mM, from a 250 mM stock in DMSO) were added as electron acceptors. The mixed

DOI: 10.1021/bi5014134
Biochemistry 2015, 54, 622−628

sample was pipetted onto the surface of the electrode and covered with a quartz coverslip creating a thin layer (<1 mm) and dark-adapted for 20 min. The electrode polarization was turned on for 90 s before each run. All experiments were performed in darkness or under dim green LED illumination (λ_{max} = 525 nm).

RESULTS

As shown in Figure 2, period-four oscillations in flash O_2 yield damp more rapidly in the presence of ammonia. This change in Kok cycle efficiency was quantified by mathematical modeling and is reported as respective miss probabilities (α) in Figure 3. The probability of misses increases with increasing temperature for both control and ammonia conditions.

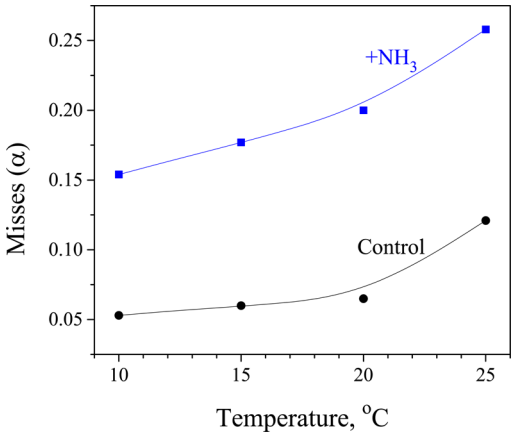

Figure 3. Dependence of the Kok model miss (α) parameter on temperature.

By varying the dark interval between the first and second flash, we monitored the rate of S_2 decay as shown in Figure 4. The decay was biphasic, and the data were fit to a two-component exponential decay function as reported in Table 1. At all temperatures studied, S_2 decays approximately 50% slower in the presence of ammonia.

The temperature dependencies of both the slow and fast components of S_2 decay are reported in an Arrhenius plot in Figure 5. Activation energies were calculated from linear fits of the slopes and are listed in Table 2. No significant variation in activation energy was observed between control and ammonia conditions. In addition, both fast and slow components of S_2 decay have similar activation energies.

DISCUSSION

To interpret our data, we introduce a kinetic model (Figure 6) that describes the pathway of S_2 formation and decay. For control conditions, the intermediates outside the dotted box were analyzed using the rate constants in Table 3 in a manner similar to that of a previous study by Styring and co-workers.[24] At 25 °C, the slow component of S_2 decay has a half-life of approximately 69.1 s (Table 1). Using the reported rate constants listed in Table 3, k_{12} was systemically varied to reproduce the observed S_2 decay half-life. An optimized k_{12} value of 114 s^{-1} provided a predicted half-life of 69.6 s.

The fast component of S_2 decay likely represents differences in the hydrogen-bonding environment of Y_Z, which in turn affects the kinetics of P^+ reduction by Y_Z (represented as k_{32} in Figure 6). Renger, Witt, and co-workers have shown that P^+ reduction occurs with three distinct kinetic phases: "fast nanosecond", "slow nanosecond", and "microsecond".[25−27] Electron transfer occurs in the nanosecond time scale in a

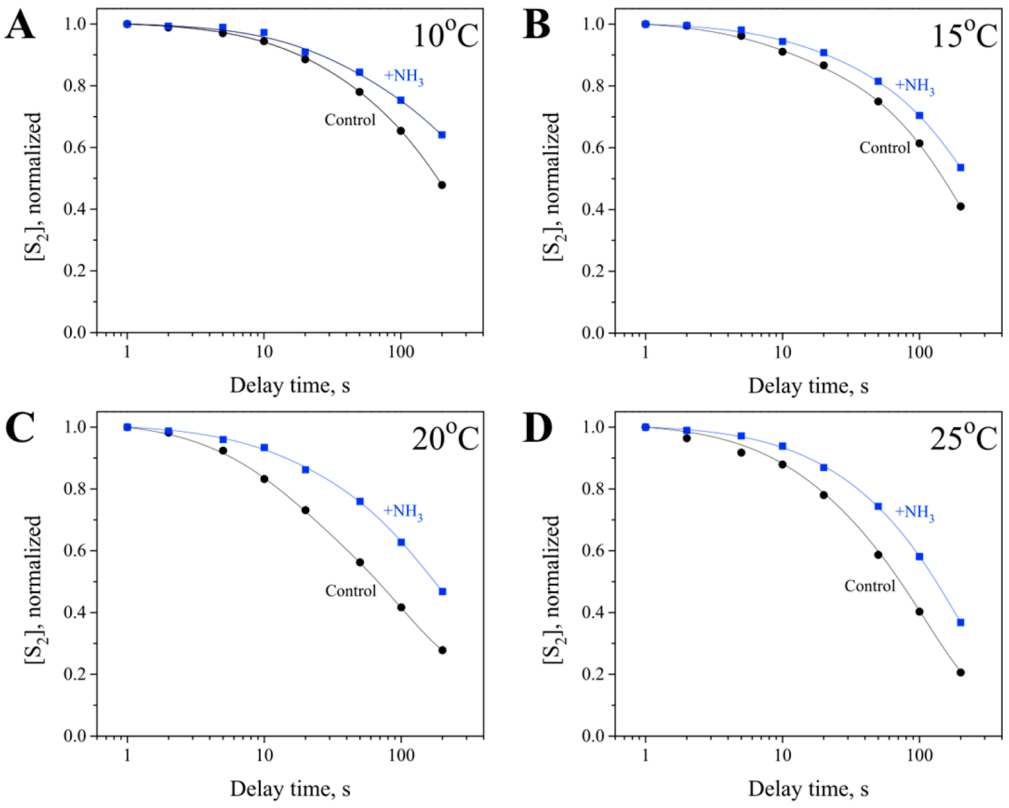

Figure 4. S_2 decay in the absence (black) and presence (blue) of ammonia at (A) 10, (B) 15, (C) 20, and (D) 25 °C.

DOI: 10.1021/bi5014134
Biochemistry 2015, 54, 622−628

Table 1. S_2 Decay Lifetimes[a]

	control				with NH_3			
	$t_{1/2}^{f}$ (s)	%	$t_{1/2}^{s}$ (s)	%	$t_{1/2}^{f}$ (s)	%	$t_{1/2}^{s}$ (s)	%
10 °C	15.2 ± 3.1	10.7	181.2 ± 26.0	89.3	21.6 ± 4.5	10.5	287.3 ± 28.5	89.5
15 °C	10.3 ± 2.6	9.3	136.0 ± 24.0	90.7	16.5 ± 2.6	7.6	198.6 ± 27.6	92.4
20 °C	8.1 ± 2.9	13.0	82.3 ± 15.5	87.0	12.8 ± 3.9	7.5	136.8 ± 29.1	92.5
25 °C	7.1 ± 2.7	11.4	69.1 ± 10.1	88.6	9.1 ± 2.7	11.4	113.2 ± 17.5	88.6

[a]Where $t_{1/2}^{f}$ and $t_{1/2}^{s}$ represent the half-times for the fast and slow components, respectively. Data from Figure 4 were fit to a two-component exponential decay model. Data represent the means of three or four replicates with the standard error.

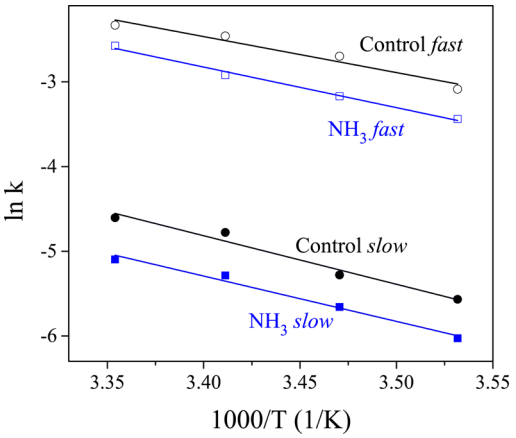

Figure 5. Arrhenius plot of temperature-dependent S_2 decay data in Figure 4 and Table 1.

Table 2. Activation Energies Derived from the Slopes of Figure 5

	E_a (kcal mol^{-1})
control fast	8.2 ± 1.7
with NH_3 fast	9.2 ± 1.0
control slow	11.1 ± 2.5
with NH_3 slow	10.3 ± 2.0

Table 3. Rate Constants for the S_2 Decay Model Presented in Figure 6[a]

		k (s^{-1})	ref
k_{34}	$Q_A^-P^+ \rightarrow Q_AP$	410	33, 41
k_{32}[b]	$P^+Y_Z \rightarrow PY_Z^\bullet$	200000	30
k_{32}[c]	$P^+Y_Z \rightarrow PY_Z^\bullet$	19800	25
k_{23}	$PY_Z^\bullet \rightarrow P^+Y_Z$	300	30
k_{21}	$Y_Z^\bullet S_1 \rightarrow Y_ZS_2$	6930	28, 42
k_{12}	$Y_ZS_2 \rightarrow Y_Z^\bullet S_1$	*114*	
k_{10}	$S_2 \rightarrow S_2^{NH_3}$	*693*	
k_{01}	$S_2^{NH_3} \rightarrow S_2$	*≤6.9*	
k_{02}	$Y_ZS_2^{NH_3} \rightarrow Y_Z^\bullet S_1$	*65*	
k_{20}	$Y_Z^\bullet S_1 \rightarrow Y_ZS_2^{NH_3}$	*≤0.7*	

[a]Values in italics are derived from this study. [b]Slow S_2 decay component (88.6% at 25 °C). [c]Fast S_2 decay component (11.4% at 25 °C).

majority of centers (80−90%), while the remaining centers have significantly slower kinetics with a half-life of 30−35 μs.[28] As previously discussed,[24,29,30] this heterogeneity in P^+ reduction kinetics gives rise to biphasic kinetics of $[Q_A^-P^+]$ charge recombination (k_{34} in Figure 6). The observed distributions of the slow and fast components of S_2 decay are 88.6 and 11.4%, respectively, under both control and ammonia conditions, which are in qualitative agreement for the populations of centers with nanosecond and microsecond P^+ reduction kinetics, respectively.

Using the calculated value of k_{12} (114 s^{-1}), k_{32} was changed from 200000 s^{-1} (fast decay component) to 19800 s^{-1} ($t_{1/2}$ = 35 μs; slow decay component). The predicted half-life of S_2 decay decreased from 69.6 to 6.8 s, which is in excellent agreement with the experimental value of 7.1 s for the control S_2 decay fast component. The solid traces in Figure 6 represent the sum of 88.6% of centers with a k_{32} of 200000 s^{-1} and 11.4% of centers with a k_{32} of 19800 s^{-1}. This analysis provides good agreement with the observed S_2 decay (represented as the increase in S_1, black dots).

For experiments including ammonia, an additional intermediate was added to the kinetic model (dotted box, $Q_A^-PY_ZS_2^{NH_3}$). A quantitative analysis is complicated by the introduction of four additional rate constants. However, EPR studies have clearly shown that $S_2^{NH_3}$ is formed by ammonia binding to S_2[8] and that $S_2^{NH_3}$ decays directly to S_1 (not via S_2).[12] Therefore, the magnitudes of k_{20} (direct formation of $S_2^{NH_3}$ from S_1) and k_{01} (release of ammonia from $S_2^{NH_3}$) are small. For all subsequent analyses, k_{20} was set to $0.01k_{02}$. An optimal value of k_{01} was found to be $0.01k_{10}$ (see discussion below). Spectroscopy also indicates that the ratio of $[S_2^{NH_3}]$ to $[S_2]$ is large (the altered multiline EPR signal is formed in high yield).[8] Herein, we assume that this ratio is at least 10:1.

As shown in Figure S1 of the Supporting Information, k_{02} has an upper limit of approximately 70 s^{-1}, which is reached when both k_{10} and k_{10}/k_{01} are large (i.e., $S_2^{NH_3}$ formation is fast and proceeds in high yield). The yield of $S_2^{NH_3}$ was also plotted as a function of k_{10} and k_{10}/k_{01} (Figure S2 of the Supporting Information). As expected, the $[S_2^{NH_3}]/[S_2]$ ratio approaches infinity as k_{10} and k_{10}/k_{01} are increased. At 25 °C, the slow component of S_2 decay in the presence of ammonia has a half-life of 113.2 s (Table 1). To reasonably reproduce this value, we propose that $S_2^{NH_3}$ formation (k_{10}) occurs with a half-life of 1 ms (693 s^{-1}) and a k_{10}/k_{01} value of 100. The corresponding rate of k_{02} that provides a net half-life for S_2 of 113.2 s is 65 s^{-1}. We note that this value is near the asymptote of Figure S1 of the Supporting Information, and the calculated yield $S_2^{NH_3}/S_2$ ratio is 10. Again, we can account for the biphasic nature of S_2 decay by changing k_{32} from 200000 to 19800 s^{-1}. When all other rates are held constant, the predicted fast component half-life is 11.1 s, which agrees well with the observed half-life of 9.1 s. The dashed traces in Figure 6 represent the sum of 88.6% of centers with a k_{32} of 200000 s^{-1} and 11.4% of centers with a k_{32} of 19800 s^{-1}. This analysis provides good agreement with the observed S_2 decay in the presence of ammonia (represented as the increase in S_1, brown dots).

Our proposed rate constant for the binding of ammonia to S_2 (k_{10}; $t_{1/2}$ = 1 ms) is faster than previous estimates[10,12] but is required to explain the high yield of $S_2^{NH_3}$ formation. As shown

DOI: 10.1021/bi5014134
Biochemistry 2015, 54, 622−628

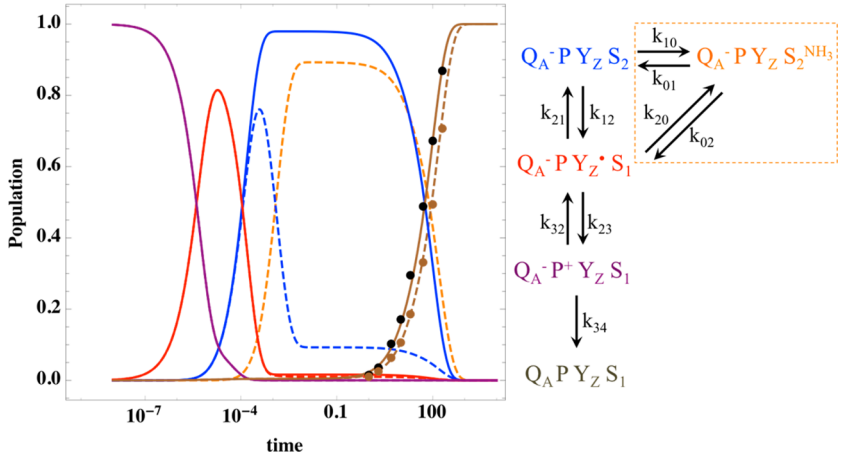

Figure 6. Kinetic model for the binding of ammonia to S_2 and the decay of ammonia-bound S_2 at 25 °C. At time zero, $[Q_A^-P^+Y_ZS_1] = 1$. Solid (control) and dashed traces (with ammonia) overlap at early time values. Colors in the plot (left) correspond to the colored text of intermediates in the scheme (right). Experimental data for S_1 populations are shown as black (control) and brown (ammonia) dots.

in Figure 6, when $Y_ZS_2^{NH3}$ decays to $Y_Z^•S_1$ (k_{02}; $t_{1/2} \approx 10$ ms), $Y_Z^•S_1$ can either form Y_ZS_2 (k_{21}; $t_{1/2} = 100$ μs) or reduce P_{680} (k_{23}; $t_{1/2} = 2.3$ ms). Clearly, Y_ZS_2 formation is favored, which in turn can bind ammonia to re-form $Y_ZS_2^{NH3}$ (k_{10}; $t_{1/2} = 1$ ms). In this cycle, slow values of k_{10} result in significant accumulation of S_2 at the expense of $S_2^{NH_3}$. Our target $S_2^{NH_3}/S_2$ value of ≥10 is conservative when compared to that from the experiment but requires that ammonia bind to S_2 with a rate constant of at least 693 s^{-1} and an equilibrium constant of at least 100.

In agreement with a previous study by Delrieu,[13] the presence of ammonia decreases the efficiency of Kok model cycling by increasing the miss parameter by 2−3-fold (Figures 2 and 3). We propose that this result is correlated with the finding by Velthuys that the $S_2 \rightarrow S_3$ transition slows from 0.4 to 13 ms in the presence of ammonia.[10] The flash O_2 yield patterns in Figure 2 were measured at a flash repetition rate of 1 Hz. Using our kinetic model for ammonia conditions (Figure 6), which assumes a charge separation efficiency of 1 at time zero, the population of $[Q_A^-PY_ZS_2^{NH3}]$ at 1 s is 0.890 and that of $[Q_A^-PY_ZS_2]$ is 0.092. Those centers without ammonia bound should advance to S_3 following the next flash with an efficiency equal to that of the control. However, centers with ammonia bound advance to S_3 more than 30-fold more slowly[10] (the mechanism for the slowing of the S_2 to S_3 transition in the presence of ammonia is not fully understood but may be a result of perturbation of the structure of the OEC or the hydrogen-bonding network around the OEC). The increase in miss probability is not due to S_2 decay in the 1 s dark time between flashes, because this decay rate is slower when ammonia is present.

Our data show that S_2 decay is approximately 50% slower in the presence of ammonia (Figure 4 and Table 1), in agreement with previous studies,[8,10,12−14] which have been explained by a lower reduction potential for $S_2^{NH_3}$ than for S_2.[12,14,15] If $k_{10}/k_{01} = 100$, and a fast equilibrium is assumed, then the resulting change in the reduction potential of S_2 upon ammonia binding would be −2.7 kcal mol^{-1}. We note that this equilibrium constant is a conservative estimate, so this would represent a lower limit.

The overall decay of S_2 to S_1 for both fast and slow components under both control and ammonia conditions occurs with activation energies of approximately 10 kcal mol^{-1} (Figure 5 and Table 2). Vass and co-workers used spinach thylakoids at pH 7.5 (no ammonia) to find activation energies of S_2 decay of 10.6 kcal mol^{-1} (fast component) and 15.0 kcal mol^{-1} (slow component).[31] These values are in good agreement with this study but are slightly lower than results of Messinger and co-workers, who used spinach thylakoids at pH 7.0 (no ammonia) and found activation energies of 13.1 kcal mol^{-1} (fast component) and 20.3 kcal mol^{-1} (slow component).[23]

S_2 decay is a multistep process, which complicates the interpretation of the observed activation energy. What is the thermodynamic rate-determining step? $[Q_A^-P^+]$ charge recombination (k_{34} in Figure 6) occurs with either no activation barrier (direct pathway) or a small activation barrier of 3−4 kcal mol^{-1} (indirect pathway).[32,33] Therefore, either $Y_Z^•$ reduction by P (k_{23} in Figure 6) or $Y_ZS_2 \rightarrow Y_Z^•S_1$ (k_{12} in Figure 6) is rate-determining. In the presence of ammonia, $S_2^{NH_3}$ primarily decays directly to $Y_Z^•S_1$ (k_{02} in Figure 6). Given that the activation barrier is the same for both control and ammonia conditions, either k_{23} is rate-determining or k_{12} and k_{02} have equivalent activation energies. The latter option, while possible, seems less likely.

Our data do not provide direct evidence of how ammonia binds to the OEC. However, we can assert that ammonia binds rapidly to S_2 ($t_{1/2} \leq 1$ ms) with a large equilibrium constant (≥100), and that k_{02} is at least 39% slower than k_{12}. These results strongly suggest that the reduction potential of $S_2^{NH_3}$ is at least 2.7 kcal mol^{-1} (120 mV) lower than that of S_2. It is highly improbable that binding of ammonia as a terminal ligand to Mn4 (replacing W1)[11] would have such an effect. The similar ligand field strengths of water and ammonia result in inorganic systems with similar reduction potentials. This difference can be estimated using "Lever parameters" that suggest a change of only 0.7 kcal mol^{-1} (30 mV).[18]

Our preferred model is one in which ammonia binds to S_2 as a bridging ligand as recently suggested by Pokhrel and Brudvig.[34] This conclusion is fully consistent with the interpretation of ESEEM[9] and FTIR[17] studies. In addition, a bridging motif (especially the possibility of a N^{3-} nitrido bridge) explains the lack of reactivity of S_2 with substituted amines,[5] and the absence of changes in protons near the OEC.[11] Such a bridging ligand would most likely replace the μ_3-oxo ligand (O5) that can be exchanged with bulk water.[35,36] The substitution of ammonia for O5 may also account for the

DOI: 10.1021/bi5014134
Biochemistry 2015, 54, 622−628

increase in a Mn−Mn distance from 2.72 to 2.87 Å as observed for ammonia-bound S_2 by EXAFS.[37]

When S_1 samples containing ammonia are illuminated at 200 K, an S_2 $g = 4.1$ EPR signal is first formed.[5] If the sample is quickly annealed to 273 K, the $g = 4.1$ signal is efficiently converted to the altered $g = 2$ multiline signal representing $S_2^{NH_3}$.[5] Alternatively, extended incubation at ∼200 K will also give rise to the multiline signal.[12] Because diffusion at 200 K is clearly limited and $S_2^{NH_3}$ formation is rapid, we propose that ammonia is "prebound" to the OEC before S_2 formation in such a way that equilibrium between the two S_2 isoforms[38] is shifted to the $g = 4.1$ state. This equilibrium is sensitive to the hydrogen-bonding network surrounding the OEC.[34] Thus, we offer two hypotheses for ammonia binding. (1) In S_1, ammonia is hydrogen bonded to terminal water(s) or oxo bridge ligands of the OEC in such a position where it can rapidly exchange upon formation of S_2, or (2) ammonia is bound as a terminal ligand to the OEC in S_1 and is rearranged to a bridging motif in S_2. Differentiating between these proposals will require further experimental evidence.

If ammonia is bound as a bridging ligand at the O5 position, O5 is then excluded as a substrate water for the O_2 release mechanism. It follows that the proposed oxo−oxyl radical coupling mechanism involving O5[1,39] is not supported by this mode of ammonia binding. We instead favor a nucleophile attack mechanism for O−O bond formation[40] involving W2 and W3, which would not be affected by substitution of ammonia for O5.[34]

■ ASSOCIATED CONTENT

Supporting Information

Two figures showing the dependencies of k_{02} and $[S_2^{NH_3}]/[S_2]$ on k_{10} and k_{10}/k_{01}. This material is available free of charge via the Internet at http://pubs.acs.org.

■ AUTHOR INFORMATION

Corresponding Author

*E-mail: gary.brudvig@yale.edu. Phone: (203) 432-5202. Fax: (203) 432-6144.

Funding

Funded by the U.S. Department of Energy, Office of Science, Office of Basic Energy Sciences (Grant DE-FG02-05ER14646).

Notes

The authors declare no competing financial interest.

■ ACKNOWLEDGMENTS

We thank Sahr Khan and Dr. Chase Zachary for helpful discussions.

■ ABBREVIATIONS

EDNMR, electron−electron double-resonance-detected nuclear magnetic resonance; ENDOR, electron nuclear double resonance; EPR, electron paramagnetic resonance; ESEEM, electron spin echo envelope modulation; EXAFS, extended X-ray absorption fine structure; FTIR, Fourier transform infrared; HEPES, 4-(2-hydroxyethyl)-1-piperazineethanesulfonic acid; OEC, oxygen-evolving complex; P_{680} (or P), primary chlorophyll *a* electron donor; PPBQ, phenyl-*p*-benzoquinone; PSII, Photosystem II; Q_A, primary plastoquinone electron acceptor; S_n, S state intermediate ($n = 0$−4); Y_Z, D1 residue tyrosine 161.

■ REFERENCES

(1) Cox, N., and Messinger, J. (2013) Reflections on substrate water and dioxygen formation. *Biochim. Biophys. Acta 1827*, 1020−1030.

(2) Vinyard, D. J., Ananyev, G. M., and Dismukes, G. C. (2013) Photosystem II: The reaction center of oxygenic photosynthesis. *Annu. Rev. Biochem. 82*, 577−606.

(3) Kok, B., Forbush, B., and McGloin, M. (1970) Cooperation of charges in photosynthetic O_2 evolution-I. A linear four step mechanism. *Photochem. Photobiol. 11*, 457−475.

(4) Forbush, B., Kok, B., and McGloin, M. P. (1971) Cooperation of charges in photosynthetic O_2 evolution-II. Damping of flash yield oscillation, deactivation. *Photochem. Photobiol. 14*, 307−321.

(5) Beck, W. F., and Brudvig, G. W. (1986) Binding of amines to the oxygen-evolving center of photosystem II. *Biochemistry 25*, 6479−6486.

(6) Sandusky, P. O., and Yocum, C. F. (1986) The chloride requirement for photosynthetic oxygen evolution: Factors affecting nucleophilic displacement of chloride from the oxygen-evolving complex. *Biochim. Biophys. Acta 849*, 85−93.

(7) Sandusky, P. O., and Yocum, C. F. (1984) The chloride requirement for photosynthetic oxygen evolution. Analysis of the effects of chloride and other anions on amine inhibition of the oxygen-evolving complex. *Biochim. Biophys. Acta 766*, 603−611.

(8) Beck, W. F., de Paula, J. C., and Brudvig, G. W. (1986) Ammonia binds to the manganese site of the oxygen-evolving complex of photosystem II in the S_2 state. *J. Am. Chem. Soc. 108*, 4018−4022.

(9) Britt, R. D., Zimmermann, J. L., Sauer, K., and Klein, M. P. (1989) Ammonia binds to the catalytic manganese of the oxygen-evolving complex of photosystem II. Evidence by electron spin-echo envelope modulation spectroscopy. *J. Am. Chem. Soc. 111*, 3522−3532.

(10) Velthuys, B. R. (1975) Binding of the inhibitor NH_3 to the oxygen-evolving apparatus of spinach chloroplasts. *Biochim. Biophys. Acta 396*, 392−401.

(11) Pérez Navarro, M., Ames, W. M., Nilsson, H., Lohmiller, T., Pantazis, D. A., Rapatskiy, L., Nowaczyk, M. M., Neese, F., Boussac, A., Messinger, J., Lubitz, W., and Cox, N. (2013) Ammonia binding to the oxygen-evolving complex of photosystem II identifies the solvent-exchangeable oxygen bridge (μ-oxo) of the manganese tetramer. *Proc. Natl. Acad. Sci. U.S.A. 110*, 15561−15566.

(12) Boussac, A., Rutherford, A. W., and Styring, S. (1990) Interaction of ammonia with the water splitting enzyme of photosystem II. *Biochemistry 29*, 24−32.

(13) Delrieu, M. J. (1976) Inhibition by ammonium chloride of the oxygen yield of photosynthesis. *Biochim. Biophys. Acta 440*, 176−188.

(14) Ono, T.-A., and Inoue, Y. (1988) Abnormal S-state turnovers in NH_3-binding Mn centers of photosynthetic O_2 evolving system. *Arch. Biochem. Biophys. 264*, 82−92.

(15) Andréasson, L.-E., Hansson, Ö., and von Schenck, K. (1988) The interaction of ammonia with the photosynthetic oxygen-evolving system. *Biochim. Biophys. Acta 936*, 351−360.

(16) Tsuno, M., Suzuki, H., Kondo, T., Mino, H., and Noguchi, T. (2011) Interaction and inhibitory effect of ammonium cation in the oxygen evolving center of Photosytem II. *Biochemistry 50*, 2506−2514.

(17) Hou, L.-H., Wu, C.-M., Huang, H.-H., and Chu, H.-A. (2011) Effects of ammonia on the structure of the oxygen-evolving complex in Photosystem II as revealed by light-induced FTIR difference spectroscopy. *Biochemistry 50*, 9248−9254.

(18) Lever, A. B. P. (1990) Electrochemical parametrization of metal complex redox potentials, using the ruthenium(III)/ruthenium(II) couple to generate a ligand electrochemical series. *Inorg. Chem. 29*, 1271−1285.

(19) Berthold, D. A., Babcock, G. T., and Yocum, C. F. (1981) A highly resolved, oxygen-evolving Photosystem II preparation from spinach thylakoid membranes. *FEBS Lett. 134*, 231−234.

(20) Beck, W. F., de Paula, J. C., and Brudvig, G. W. (1985) Active and resting states of the oxygen-evolving complex of photosystem II. *Biochemistry 24*, 3035−3043.

(21) Vinyard, D. J., Zachary, C. E., Ananyev, G., and Dismukes, G. C. (2013) Thermodynamically accurate modeling of the catalytic cycle of

DOI: 10.1021/bi5014134
Biochemistry 2015, 54, 622−628

photosynthetic oxygen evolution: A mathematical solution to asymmetric Markov chains. *Biochim. Biophys. Acta 1827*, 861−868.
(22) Joliot, P., and Kok, B. (1975) Oxygen evolution in photosynthesis. In *Bioenergetics of Photosynthesis* (Govindjee, Ed.) pp 387−412, Academic Press, New York.
(23) Messinger, J., Schroeder, W. P., and Renger, G. (1993) Structure-function relations in photosystem II. Effects of temperature and chaotropic agents on the period four oscillation of flash-induced oxygen evolution. *Biochemistry 32*, 7658−7668.
(24) Chen, G., Han, G., Göransson, E., Mamedov, F., and Styring, S. (2012) Stability of the S_3 and S_2 state intermediates in Photosystem II directly probed by EPR spectroscopy. *Biochemistry 51*, 138−148.
(25) Eckert, H. J., and Renger, G. (1988) Temperature dependence of P_{680}^+ reduction in O_2-evolving PS II membrane fragments at different redox states S_i of the water oxidizing system. *FEBS Lett. 236*, 425−431.
(26) Renger, G. (1983) Biological energy conservation. In *Biophysics* (Hoppe, W., Lohmann, W., Markl, H., and Ziegler, H., Eds.) pp 347−371, Springer, Berlin.
(27) Brettel, K., Schlodder, E., and Witt, H. T. (1984) Nanosecond reduction kinetics of photooxidized chlorophyll-a_{II} (P680) in single flashes as a probe for the electron pathway, H^+-release and charge accumulation in the O_2-evolving complex. *Biochim. Biophys. Acta 766*, 403−415.
(28) Renger, G., and Weiss, W. (1986) Functional and structural aspects of photosynthetic water oxidation. *Biochem. Soc. Trans. 14*, 17−20.
(29) Buser, C. A., Diner, B. A., and Brudvig, G. W. (1992) Photooxidation of cytochrome b_{559} in oxygen-evolving Photosystem II. *Biochemistry 31*, 11449−11459.
(30) Buser, C. A., Thompson, L. K., Diner, B. A., and Brudvig, G. W. (1990) Electron-transfer reactions in manganese-depleted photosystem II. *Biochemistry 29*, 8977−8985.
(31) Vass, I., Deák, Z., and Hideg, É. (1990) Charge equilibrium between the water-oxidizing complex and the electron donor tyrosine-D in Photosystem II. *Biochim. Biophys. Acta 1017*, 63−69.
(32) Rappaport, F., Guergova-Kuras, M., Nixon, P. J., Diner, B. A., and Lavergne, J. (2002) Kinetics and pathways of charge recombination in Photosystem II. *Biochemistry 41*, 8518−8527.
(33) Reinman, S., and Mathis, P. (1981) Influence of temperature on Photosystem II electron transfer reactions. *Biochim. Biophys. Acta 635*, 249−258.
(34) Pokhrel, R., and Brudvig, G. W. (2014) Oxygen-evolving complex of photosystem II: Correlating structure with spectroscopy. *Phys. Chem. Chem. Phys. 16*, 11812−11821.
(35) McConnell, I. L., Grigoryants, V. M., Scholes, C. P., Myers, W. K., Chen, P.-Y., Whittaker, J. W., and Brudvig, G. W. (2012) EPR−ENDOR characterization of (^{17}O, ^1H, ^2H) water in manganese catalase and its relevance to the oxygen-evolving complex of Photosystem II. *J. Am. Chem. Soc. 134*, 1504−1512.
(36) Rapatskiy, L., Cox, N., Savitsky, A., Ames, W. M., Sander, J., Nowaczyk, M. M., Rögner, M., Boussac, A., Neese, F., Messinger, J., and Lubitz, W. (2012) Detection of the water-binding sites of the oxygen-evolving complex of Photosystem II using W-band ^{17}O electron−electron double resonance-detected NMR spectroscopy. *J. Am. Chem. Soc. 134*, 16619−16634.
(37) Dau, H., Andrews, J. C., Roelofs, T. A., Latimer, M. J., Liang, W., Yachandra, V. K., Sauer, K., and Klein, M. P. (1995) Structural consequences of ammonia binding to the manganese center of the photosynthetic oxygen-evolving complex: An X-ray absorption spectroscopy study of isotropic and oriented Photosystem II particles. *Biochemistry 34*, 5274−5287.
(38) Pantazis, D. A., Ames, W., Cox, N., Lubitz, W., and Neese, F. (2012) Two interconvertible structures that explain the spectroscopic properties of the oxygen-evolving complex of Photosystem II in the S_2 state. *Angew. Chem., Int. Ed. 51*, 9935−9940.
(39) Siegbahn, P. E. M. (2011) Recent theoretical studies of water oxidation in photosystem II. *J. Photochem. Photobiol., B 104*, 94−99.
(40) McEvoy, J. P., and Brudvig, G. W. (2006) Water-splitting chemistry of Photosystem II. *Chem. Rev. 106*, 4455−4483.
(41) Hillmann, B., and Schlodder, E. (1995) Electron transfer reactions in Photosystem II core complexes from *Synechococcus* at low temperature: Difference spectrum of P_{680}^+ Q_A^-/P_{680} Q_A at 77 K. *Biochim. Biophys. Acta 1231*, 76−88.
(42) Hoganson, C. W., and Babcock, G. T. (1988) Electron-transfer events near the reaction center in oxygen-evolving photosystem II preparations. *Biochemistry 27*, 5848−5855.
(43) Pal, R., Negre, C. F. A., Vogt, L., Pokhrel, R., Ertem, M. Z., Brudvig, G. W., and Batista, V. S. (2013) S_0-state model of the oxygen-evolving complex of Photosystem II. *Biochemistry 52*, 7703−7706.

DOI: 10.1021/bi5014134
Biochemistry 2015, 54, 622−628